Austenitic stainless steel is the most commonly used material in the production of orthopedic prostheses. In this study, AISI 430 SS (0.12 wt. % C; 1 wt. % Si; 1 wt. % Mn; 18 wt. % Cr; 0.04 wt. % P and 0.03 wt. % S) will be modified by creating austenite and removing its ferromagnetic properties via the high-temperature gas nitriding process. Cold rolling with various percentage reduction (30, 50, and 70 %) was followed by gas nitriding at a temperature of 1200 °C with holding times of 5, 7, and 9 hours, then quenching in water was carried out on as-annealed AISI 430 SS. The formation of the austenite phase was examined by XRD (x-ray diffraction). The microstructure and element dispersion were observed using SEM-EDS (scanning electron microscope-energy dispersive spectrometry), whereas the mechanical properties after gas nitriding and water quenching were determined by Vickers microhardness testing. At all stages of the gas nitriding process, the FCC iron indicated the austenite phase was visible on the alloy's surface, although the ferrite phase is still present. The intensity of austenite formation is produced by cold rolling 70 % reduction with a 5-hour gas nitriding time. Furthermore, the nitrogen layer was formed with a maximum thickness layer of approximately 3.14 µm after a 50 % reduction in cold rolling and 9 hours of gas nitriding process followed by water quenching. The hardness reached 600 HVN in this condition. This is due to the distribution of carbon that is concentrated on the surface. As the percent reduction in the cold rolling process increases, the strength of AISI 430 SS after gas nitriding can increase, causing an increase in the number of dislocations. The highest tensile strength and hardness of AISI 430 SS of 669 MPa and 271.83 HVN were obtained with a reduction of 70 %

Keywords: AISI 430 SS, austenite, high-temperature gas nitriding, cold rolling, nitrogen layer

THE EFFECT OF COLD ROLLING AND HIGH-TEMPERATURE GAS NITRIDING ON AUSTENITE PHASE FORMATION IN AISI 430 SS

Ika Kartika
Corresponding author
Doctor of Material Processing, Senior Researcher*
E-mail: ikak001@lipi.go.id
Kevin Kurnia
Bachelor of Engineering, Master of Engineering,
Junior Researcher***
Galih Senopati
Junior Researcher*
Joko Triwardono
Technical Supervisi*
Bambang Hermanto
Junior Researcher
Research Center for Physic**
Fendy Rokhmanto
Junior Researcher*
Made Subekti Dwijaya
Junior Researcher*
Alfirano
Doctor of Material Engineering, Professor***
*Research Center for Metallurgy and Materials**
**Indonesian Institute of Sciences (LIPI)
Building 470, Puspiptek Serpong,
Tangerang Selatan, Banten, Indonesia, 15314
***Department of Metallurgy Engineering
Sultan Ageng Tirtayasa University
Jl. Jenderal Sudirman Km. 3, Cilegon, Banten, Indonesia, 42435

1. Introduction

In comparison to other materials such as polymers and ceramics, metallic materials are the most commonly used for biomedical applications due to their high mechanical properties, biocompatibility, and corrosion resistance [1, 2]. Stainless steel (SS) 316L is the most widely used and has been used for a long time among other metallic materials such as titanium and cobalt alloy, such as bone plates, screws, spinal fixations, stents, guidewires, and dental implants [3]. Stainless steel 316 L has good mechanical properties, corrosion resistance, machinability and formability, and a low manufacturing cost [4]. However, the nickel element in SS 316L has a negative impact on the human body over time, causing irritation and even cancer. Nickel can be liberated from

stainless steel 316L implant devices due to corrosion, wear, or other factors. Nickel, which acts as an allergen, may cause inflammation, skin irritation, allergy reactions, teratogenicity, and carcinogenicity [5]. In recent years, nickel-free stainless steel is thought as a potential biomedical device to replace SS 316L [6–9].

Nickel element in austenitic stainless steel can be substituted by nitrogen or manganese or both [10]. Nitrogen is known as an austenite stabilizing element, can increase strength and corrosion resistance in stainless steel [11, 12]. High nitrogen austenitic stainless steel (HNSs) can be obtained by pressurized electroslag remelting process (PESR) and mechanical alloying [11]. To obtain stainless steel with a homogeneous microstructure, it is necessary to notice the right nitrogen content so that there is no depletion of chromi-

um metal that causes local corrosion in certain areas [13]. In recent years, a new method has been developed to obtain nickel-free stainless steel with nitrogen gas adsorption treatment using free-nickel ferritic stainless steel as raw material [14]. Manufacturers can use common ferritic stainless steel, which is much lower-cost than austenitic stainless steel by modifying the microstructure using nitrogen gas adsorption.

2. Literature review and problem statement

AISI 430 SS is a common raw material used in the production of nickel-free austenitic stainless steel. AISI 430 SS has a magnetic ferrite phase and has a lower strength and corrosion resistance value than SS 316L. Nevertheless, nickel-free ferritic or martensitic stainless steel is ferromagnetic and has a lack of ductility [15]. As a result, certain manufacturing processes are required to improve mechanical properties and corrosion resistance, as well as change the ferrite phase to austenite in AISI 430 SS.

The properties of the nitrogen adsorbed on the ferritic Fe-23 wt. %Cr powder alloy were investigated. In this study, the nitriding process is extremely effective for improving the mechanical properties of ferritic stainless steels. Because nitrogen can activate the mechanism of solid solution strengthening, it improves mechanical properties. However, the sintering temperature was used in this study for nitrogen absorption [16].

In other studies, nitrogen addition to Fe-24Cr and Fe-24Cr-2Mo improved corrosion resistance by converting the ferrite phase to a more stable austenite phase. The cold working process, in addition to nitriding, can improve the mechanical properties of stainless steel by increasing the number of dislocations [14]. The addition of nitrogen in HNSs results in a strengthening mechanism that includes pinning and unpinning the nitrogen atom's dislocation [5]. Short-range ordering of substitutional and interstitial elements (such as Cr-N) may help to strengthen N-containing stainless steels [17]. Forging or rolling are two cold working processes commonly used in the production of nickel-free austenitic stainless steel [14]. Furthermore, to understand the effects of grain refinement on nitrogen absorption, Fe-24Cr-2Mo fine grains generated by hot forging and cold forging were evaluated both before and after nitrogen absorption treatment. As a result, grain refinement prior to nitrogen absorption treatment improves the mechanical properties of nickel-free austenitic stainless steel [18].

The effect of the manufacturing process on changes in the oxide layer using Hank's solution has been studied in Fe-24Cr-2Mo-1N, Fe-26.7Cr-1.1Mo3.6N, and Fe-24Cr-2Mo-1.4N. The first two alloys are made with nitrogen absorption treatment after machining, while the third alloy is made with the nitrogen gas-pressurized electro-slug remelting process. This study concludes that all of the alloys would have a higher pitting corrosion resistance because of nitrogen absorption. This condition is most likely to be expected in the human body following implantation [19].

All of the preceding information explains how work-forming and nitriding processes can improve the mechanical properties of ferritic materials. However, little attention has been paid to the use of AISI 430 SS in prosthetic implants. This is an impressive result that can be achieved in the implant field's research environment, which can use low-cost materials as implant prosthesis materials. The primary goal is to convert the ferrite structure in AISI 430 SS to austenite, which is a challenging process with few references. Furthermore, given the properties of the ferritic materials, the formation of the nitride layer is an equally important goal. It is significant because the ferrite structure is ferromagnetic, in addition to lacking other properties such as low mechanical properties and corrosion resistance. As a result, it is intriguing to investigate AISI 430 SS as an implant prosthesis material using various deformation techniques such as cold rolling, high-temperature gas nitriding, and water quenching.

3. The aim and objectives of the study

The aim of this study is to investigate the microstructure and mechanical properties of AISI 430 SS after cold rolling in various deformation, high-temperature gas nitriding, and water quenching. If the entire process flow is followed to achieve the desired result, AISI 430 SS is very likely to be used as a replacement material for prosthesis implants.

To achieve this aim, the following objectives are accomplished:

– to assess the effectiveness of the cold rolling process with deformation variations, high-temperature gas nitriding, and water quenching on the formation of the austenite phase in AISI 430 ferritic stainless steel;

– to determine the relationship between the thickness of the nitride layer formed after the entire process and the resulting mechanical properties in AISI 430 ferritic stainless steel, as a result of which the material is qualified as an implant prosthesis material.

4. Materials and methods

In this study, AISI 430 SS was used as the raw material, and the chemical composition is shown in Table 1.

Table 1

Chemical composition of AISI 430 SS

Element	Wt. %
C	0.12
Si	1
Mn	1
P	0.04
S	0.03
Cr	18

A 3 mm thick abrasive cutting wheel was used to section the stainless steel AISI 430 SS. The plate was cold-rolled at various reductions (30, 50 and 70 %). Following the gas nitriding process, the as-rolled AISI 430 SS is cut for tensile test sample profile according to ASTM E8 standard. The 99.99 % pure nitrogen is used for the nitriding process. The gas nitriding process is carried out in a tube furnace at 1,200 °C for 5 to 9 hours at a time. The vacuum is turned on for 15 minutes before the process begins to clear it of any other gas contamination. The AISI 430 SS sample was rapidly cooled (quenched) with water after the gas nitriding process.
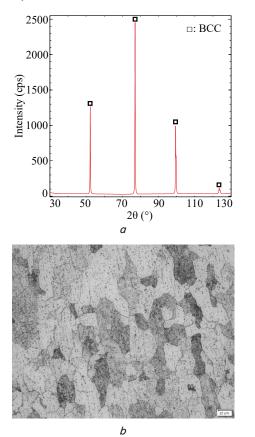
The AISI 430 SS plate was sanded with grit sandpaper 400, 600, 800, 1,000, 1,200, 1,500, and 2,000 for microstructural examination, then polished with Al_2O_3 paste with a roughness of 0.1μ and cleaned with water and ethanol. Aqua regia was then used to etch the sample. Olympus optical

microscopes and SEM-EDS (scanning electron microscope – energy dispersive spectrometry) were used to examine the microstructure. To analyze their phases, XRD (x-ray diffraction) measurements were performed at room temperature using a Bruker diffractometer equipped with a Co K radiation source and operating at 30 kV and 15 mA.
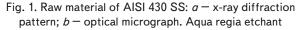
The tensile test is used to determine the material's strength before and after the nitriding process. The ASTM E8 standard is used for the tensile test profile standard, with a maximum load of 70 kN and a speed of 0.635 mm/second using a Tinius Olsen brand tool. Hardness testing was performed on stainless steel AISI 430 ferritic specimens before and after the nitriding process to determine the hardness value. The load was applied for 15 seconds at 300 gf using a Vickers microhardness tester Mitutoyo HM-200.

5. Results of examination of composition, microstructure and mechanical properties of AISI 430 ferritic stainless steel after the entire process

5. 1. Results of the raw material examination

Fig. 1, *a* shows the results of XRD (x-ray diffraction) analysis, while Fig. 1, *b* depicts the optical micrograph of AISI 430 SS prior to the gas nitriding process (raw material).

a

b

Fig. 1. Raw material of AISI 430 SS: *a* — x-ray diffraction pattern; *b* — optical micrograph. Aqua regia etchant

The x-ray diffraction pattern in Fig. 1, *a* shows all diffraction peaks were identified as α (ferrite) with bcc (body centered cubic) structure. Fig. 1, *b* depicts the microstructure of AISI 430 SS, which is composed of equiaxed ferrite grains and some inclusions.

5. 2. XRD results following gas nitriding

Fig. 2, *a–c* depicts the diffraction pattern of AISI 430 SS after cold rolling with various thickness reductions (30, 50, and 70 %) followed by a nitriding process at 1,200 °C for 5 and 9 hours before quenching in water.

As shown in Fig. 2, *a–c*, the γ-phase (austenite) is observed in all conditions, indicating that the γ-austenite phase occurred after the gas nitriding process and that the α-ferrite phase was also observed. At all holding times of the gas nitriding process, the γ-phase can be seen at angles 2θ=51°, 59°, 89°, 111°, and 119°.
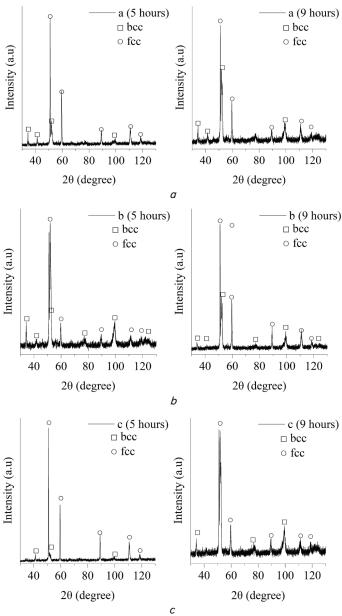

a

b

c

Fig. 2. Diffraction pattern of AISI 430 SS after cold rolling and nitriding *T*=1200 °C for 5 and 9 hours with reduction of (%): *a* — 30; *b* — 50; *c* — 70

Fig. 3, *a–c* shows a cross-sectional SEM image of AISI 430 SS after cold rolling (30, 50, and 70 % reduction) and gas nitriding at 1,200 °C for 9 hours, followed by quenching in water media. The white layer on the surface of AISI 430 SS indicated the nitride layer, and the austenite phase was also observed close to the white layer.

The distribution of elements on the surface of AISI 430 SS after cold rolling with reduction variations and the nitriding process followed by quenching is depicted in Fig. 4, $a–c$.
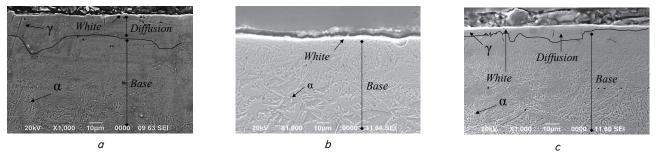

Fig. 3. SEM results of AISI 430 SS after cold rolling and nitriding T=1,200 °C − 9 hours continued quenching in water, with rolling reduction (%): a − 30; b − 50; c − 70 %. Etched aqua regia
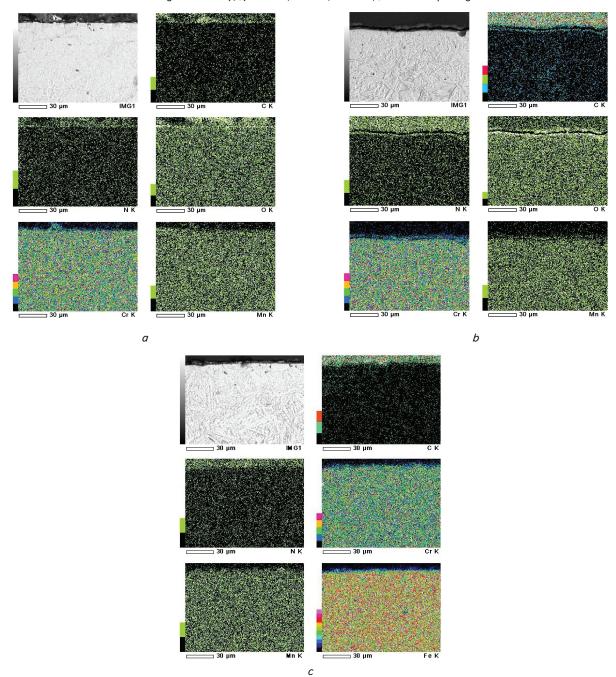

Fig. 4. SEM results of elemental distribution on AISI 430 SS after cold rolling and nitriding T=1,200 °C − 9 hours with reduction variations (%): a − 30; b − 50; c − 70. Etching aqua regia

C, N, Cr, Mn, and Fe elements were subjected to SEM-EDS mapping in AISI 430 SS. The color next to the image indicates the intensity of the element distribution (Fig. 4, *a−c*).

The ultimate tensile strength of AISI 430 SS after various deformations, gas nitriding, and water quenching is shown in Fig. 5. The A0; A1; A2; and A3 samples have a cold-roll reduction of 30% with 0; 5; 7; and 9 hours of gas nitriding, respectively. While the B0; B1; B2; B3 samples have a 50% reduction with a 0; 5; 7; 9 hours gas nitriding, the C0; C1; C2; C3 samples have a 70% cold-roll reduction with a 0; 5; 7; 9 hours gas nitriding.
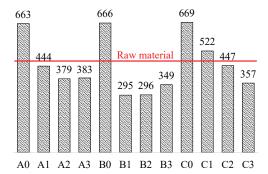
Fig. 5. Tensile strength of AISI 430 SS with various deformations of cold rolling, gas nitriding, and water quenching

Fig. 6, *a−c* shows the SEM fractography image of AISI 430 SS after tensile testing. Fig. 6, *a* depicts the SEM result of an AISI 430 SS fracture without treatment.

Fig. 6, *a* shows a dimple fracture, which is distinguished by the presence of cups on the fracture surface. Fig. 6, *b, c* shows the fractography image by SEM after gas-nitrided for 9 hours and deformed by 50 % and 70 %, respectively.
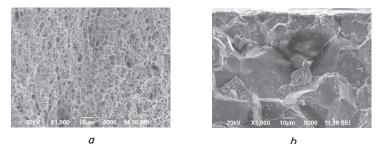
Table 2 shows the hardness values of AISI 430 SS without treatment and the material subjected to reduction.

Table 2

Hardness value (HVN) of AISI 430 SS

Process Parameter	Hardness Value (HVN)
Raw Material	164
Cold-Rolled 30 %	252
Cold-Rolled 50 %	268
Cold-Rolled 70 %	272

Fig. 7, *a−c* depicts the deep profile of microhardness of AISI 430 SS after the entire process is completed, with reductions during cold rolling of 30, 50, and 70 %. Hardness values were measured every 100 μm from the alloy surface to a depth of 600 μm.

Fig. 7, *a−c* depicts the deep profile of microhardness of AISI 430 SS after the entire process is completed, with reductions during cold rolling of 30, 50, and 70 %. Hardness values were measured every 100 μm from the alloy surface to a depth of 600 μm.
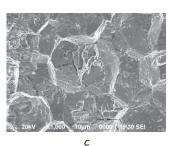

Fig. 6. SEM fractography results of AISI 430 after the tensile test: *a* — raw material; *b* — 50 % reduction — 9 hours nitriding; *c* — 70 % reduction — 9 hours nitriding
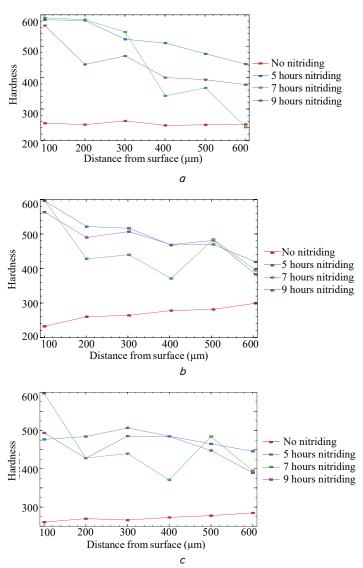

Fig. 7. AISI 430 SS microhardness after gas nitriding with cold rolling reductions (%) of: *a* — 30; *b* — 50; *c* — 70

6. Discussion of composition, microstructure and mechanical properties of AISI 430 ferritic stainless steel after the entire process

The XRD profile and optical microscopy image in Fig. 1, *a*, *b* show that the AISI 430 SS used in this study has only a ferrite phase with a BCC (body-centered cubic) unit cell. Stainless steel with high chromium (18 wt. %) content will form a stable and homogenous ferritic structure [6].

On the other hand, as shown in Fig. 2, *a–c*, the austenite was formed after the nitrogen adsorption process. There is also a diffraction pattern of the α-phase with BCC (body-centered cubic) unit cells, indicating that the ferrite phase is still present on the surface of AISI 430 SS. According to the XRD profile, no CrN or Cr_2N was detected with nitrogen absorption, indicating that no nitride was formed in AISI 430 SS (Fig. 2, *a–c*).

As shown in Fig. 3, *a–c*, a nitride layer of a certain thickness is formed on the surface of the alloy after gas nitriding. When cold rolling of AISI 430 SS with a 30 % reduction, the thickness of the nitriding layer formed was 0.836 µm (Fig. 3, *a*), with a 50 % reduction, the thickness of the nitriding layer formed was 3.140 µm (Fig. 3, *b*), and with a 70 % reduction, the thickness of the nitriding layer formed was 1.122 µm (Fig. 3, *c*). After a 50 % reduction, the AISI 430 SS had the thickest nitriding layer, possibly due to the distribution of concentrated carbon on the surface of the AISI 430 SS. With a 50 % reduction in cold rolling, the C, N, Mn, and Cr elements are evenly distributed, and the nitriding layer is very significant (Fig. 4, *b*). Nitrogen solubility can be reduced as carbon content increases. The decrease in nitrogen solubility may result in the formation of pearlite nitride precipitates at grain boundaries [15, 20]. The presence of acicular ferrite and martensite was observed in the base metal area after a 50 % reduction of cold rolling with gas nitriding holding time of 7 to 9 hours (Fig. 4, *b*, *c*). Also, solute manganese inhibits the formation of polygonal ferrite and pearlite, which promotes the formation of acicular ferrite. Otherwise, Mn diffusion in austenite influences austenite formation, where the austenite phase formation is proportional to the area of the Mn depleted zone. The ferrite nucleation energy should be reduced to produce austenite stabilization by increasing the area with sufficient manganese content [21, 22].

The initial strength of AISI 430 SS is 469 MPa, which differs slightly from 450 MPa (ASTM A240). Fig. 5 shows the tensile strength of AISI 430 SS after various processes. The strength value of AISI 430 SS increased significantly after cold-rolled by 30 % (A0), 50 % (B0), and 70 % (C0). As the percentage reduction in cold rolling increases, the strength of the metal increases, as does the number of dislocations. The number of dislocations in a metal can be increased to increase its strength value. However, as the reduction in the cold rolling process increases, the number of dislocations increases, which reduces the elasticity of the AISI 430 SS [23].

The tensile strength of AISI 430 SS was reduced after the nitriding process was completed. This is because increasing the heating time expands the grain size and reduces the number of dislocations. The number of dislocations in AISI 430 SS can be reduced to reduce its strength value. The increased holding time of the nitriding process, on the other hand, causes an increase in the strength value at AISI 430 SS with a 50 % reduction. This is due to the lengthening of the nitriding process, which results in an increase in nitrogen content, which diffuses into AISI 430 SS. On the other hand, nitrogen solubilities in various iron modifications are proportional to $\sqrt{\rho}$, where ρ is pressure, indicating that nitrogen dissolves as a single atom rather than diatomic molecules. The very low solubility of nitrogen in contact with iron at 1-atmosphere pressure is due, in part, to the fact that the gas is almost entirely composed of diatomic molecules, with comparatively few free atoms of nitrogen striking the solid's surface [24]. As a result, nitrogen is unlikely to form as a precipitate in this study.

The high chromium content of AISI 430 SS causes this ductile fracture (16–18 % by weight) as shown in Fig. 6, *a*. The presence of chromium in steel can reduce its hardness value while increasing its elongation [1]. The intergranular fracture was discovered to have a small cleavage facet on the surface of many grains, whereas the grain structure causes the fracture to be relatively rough due to embrittlement, with voids caused by chromium carbide precipitates and inclusions (Fig. 6, *b*, *c*).

After all processes are completed, the microhardness on the alloy surface increases significantly, then decreases to a depth of 600 µm (Fig. 7, *a–c*). As can be seen in Fig. 7, *a–c*, in general, the highest hardness was obtained after 7 hours of gas nitriding and the lowest hardness was obtained after 9 hours of nitriding at a 50 % reduction. As the distance between the hardness measurement and the surface increases, the hardness value of AISI 430 SS decreases. This is due to a decrease in the volume fraction of austenite in the middle of AISI 430 SS, where the austenite phase is harder than the ferrite phase [25]. The highest average hardness value is found in AISI 430 SS with a 70 % reduction. This is due to an increase in size reduction, which causes an increase in the number of dislocations in AISI 430 SS; this increase in the number of dislocations can raise the material hardness value [26].

In all parameters tested, the addition of nitrogen in the material causes a phase change from ferrite to austenite. Furthermore, this demonstrates that there has been a process of diffusion of nitrogen gas into AISI 430 stainless steel, as indicated by a nitride layer on the material's surface. However, this study has a limitation. The nitrogen solubility in the material is strongly influenced by the nitrogen gas pressure parameter. This condition will indicate the presence of dissolved nitrogen as a single atom, and not as a diatomic molecule. For this research to move forward, the parameters for applying nitrogen gas pressure must be determined. As an example, applying high pressure to the area of the material where the ammonia decomposition process occurs will have a significant impact on the increase in high nitrogen solubility.

7. Conclusions

1. The nitriding process's holding time can influence the formation of the austenitic phase in AISI 430 SS. The highest peak intensity of austenite is obtained when AISI 430 SS is subjected to a 70 % reduction and nitrided for 5 hours.

2. The percentage reduction of cold-rolled before gas nitriding affects the thickness of the nitride layer and the

mechanical properties of AISI 430 SS. The optimum nitride layer formed after a 50 % reduction in cold rolling and a nitriding holding time of 9 hours was 3.14 µm with a hardness value of 600 HVN. The greatest tensile strength and hardness were obtained with a 70 % reduction of 669 MPa and 271.83 HVN, respectively.

References

1. Sumita, M., Hanawa, T., Teoh, S. H. (2004). Development of nitrogen-containing nickel-free austenitic stainless steels for metallic biomaterials – review. Materials Science and Engineering: C, 24 (6-8), 753–760. doi: https://doi.org/10.1016/j.msec.2004.08.030

2. Sutowo, C., Senopati, G., W Pramono, A., Supriadi, S., Suharno, B. (2020). Microstructures, mechanical properties, and corrosion behavior of novel multi-component Ti-6Mo-6Nb-xSn-xMn alloys for biomedical applications. AIMS Materials Science, 7 (2), 192–202. doi: https://doi.org/10.3934/matersci.2020.2.192

3. Black, J., Hastings, G. (1998). Handbook of Biomaterial Properties. Springer, 590. doi: https://doi.org/10.1007/978-1-4615-5801-9

4. Niinomi, M., Nakai, M., Hieda, J. (2012). Development of new metallic alloys for biomedical applications. Acta Biomaterialia, 8 (11), 3888–3903. doi: https://doi.org/10.1016/j.actbio.2012.06.037

5. Yang, K., Ren, Y. (2010). Nickel-free austenitic stainless steels for medical applications. Science and Technology of Advanced Materials, 11 (1), 014105. doi: https://doi.org/10.1088/1468-6996/11/1/014105

6. Berton, E. M., Neves, J. C. K., Mafra, M., Borges, P. C. (2017). Nitrogen enrichment of AISI 409 stainless steel by solution heat treatment after plasma nitriding. Metallic Materials, 55 (05), 317–321. doi: https://doi.org/10.4149/km_2017_5_317

7. Li, J., Yang, Y., Ren, Y., Dong, J., Yang, K. (2018). Effect of cold deformation on corrosion fatigue behavior of nickel-free high nitrogen austenitic stainless steel for coronary stent application. Journal of Materials Science & Technology, 34 (4), 660–665. doi: https://doi.org/10.1016/j.jmst.2017.10.002

8. Mola, J., Ullrich, C., Kuang, B., Rahimi, R., Huang, Q., Rafaja, D., Ritzenhoff, R. (2017). Austenitic Nickel- and Manganese-Free Fe-15Cr-1Mo-0.4N-0.3C Steel: Tensile Behavior and Deformation-Induced Processes between 298 K and 503 K (25 °C and 230 °C). Metallurgical and Materials Transactions A, 48 (3), 1033–1052. doi: https://doi.org/10.1007/s11661-017-3960-x

9. Aydin, H., Bayram, A., Topçu, Ş. (2013). Friction Characteristics of Nitrided Layers on AISI 430 Ferritic Stainless Steel Obtained by Various Nitriding Processes. Materials Science, 19 (1). doi: https://doi.org/10.5755/j01.ms.19.1.3819

10. Patnaik, L., Ranjan Maity, S., Kumar, S. (2020). Status of nickel free stainless steel in biomedical field: A review of last 10 years and what else can be done. Materials Today: Proceedings, 26, 638–643. doi: https://doi.org/10.1016/j.matpr.2019.12.205

11. Talha, M., Behera, C. K., Sinha, O. P. (2013). A review on nickel-free nitrogen containing austenitic stainless steels for biomedical applications. Materials Science and Engineering: C, 33 (7), 3563–3575. doi: https://doi.org/10.1016/j.msec.2013.06.002

12. Lo, K. H., Shek, C. H., Lai, J. K. L. (2009). Recent developments in stainless steels. Materials Science and Engineering: R: Reports, 65 (4-6), 39–104. doi: https://doi.org/10.1016/j.mser.2009.03.001

13. Feng, H., Jiang, Z., Li, H., Lu, P., Zhang, S., Zhu, H. et. al. (2018). Influence of nitrogen on corrosion behaviour of high nitrogen martensitic stainless steels manufactured by pressurized metallurgy. Corrosion Science, 144, 288–300. doi: https://doi.org/10.1016/j.corsci.2018.09.002

14. Kuroda, D., Hanawa, T., Hibaru, T., Kuroda, S., Kobayashi, M., Kobayashi, T. (2003). New Manufacturing Process of Nickel-Free Austenitic Stainless Steel with Nitrogen Absorption Treatment. MATERIALS TRANSACTIONS, 44 (3), 414–420. doi: https://doi.org/10.2320/matertrans.44.414

15. Zhang, S., Yu, Y., Wang, S., Li, H. (2017). Effects of cerium addition on solidification structure and mechanical properties of 434 ferritic stainless steel. Journal of Rare Earths, 35 (5), 518–524. doi: https://doi.org/10.1016/s1002-0721(17)60942-6

16. Nakamura, N., Takaki, S. (1996). Structural Control of Stainless Steel by Nitrogen Absorption in Solid State. ISIJ International, 36 (7), 922–926. doi: https://doi.org/10.2355/isijinternational.36.922

17. Saller, G., Spiradek-Hahn, K., Scheu, C., Clemens, H. (2006). Microstructural evolution of Cr–Mn–N austenitic steels during cold work hardening. Materials Science and Engineering: A, 427 (1-2), 246–254. doi: https://doi.org/10.1016/j.msea.2006.04.020

18. Kuroda, D., Hanawa, T., Hibaru, T., Kuroda, S., Kobayashi, M. (2003). Mechanical Properties of Thin Wires of Nickel-Free Austenintic Stainless Steel with Nitrogen Absorption Treatment. MATERIALS TRANSACTIONS, 44 (8), 1577–1582. doi: https://doi.org/10.2320/matertrans.44.1577

19. Kuroda, D., Takemoto, S., Hanawa, T., Asami, K. (2003). Characterization of the Surface Oxide Film on an Fe-Cr-N System Alloy in Environments Simulating the Human Body. MATERIALS TRANSACTIONS, 44 (12), 2664–2670. doi: https://doi.org/10.2320/matertrans.44.2664

20. Ritzenhoff, R., Hah, A. (2012). Corrosion resistance of High nitrogen steels. Corrosion Resistance. doi: https://doi.org/10.5772/33037

21. Loder, D., Michelic, S. K., Bernhard, C. (2017). Acicular Ferrite Formation and Its Influencing Factors-A Review. Journal of Materials Science Research, 6 (1), 24. doi: https://doi.org/10.5539/jmsr.v6n1p24

22. Garcia-Gonzalez, J. E. (2005). Fundamental Study on the Austenite Formation and Decomposition of low-Si, Al added Nb-Mo TRIP steels. University of Pittsburgh, 190. Available at: http://d-scholarship.pitt.edu/6715/

23. Hedayati, A., Najafizadeh, A., Kermanpur, A., Forouzan, F. (2010). The effect of cold rolling regime on microstructure and mechanical properties of AISI 304L stainless steel. Journal of Materials Processing Technology, 210 (8), 1017–1022. doi: https://doi.org/10.1016/j.jmatprotec.2010.02.010

24. Hume-Rothery, W. (1966). The structures of Alloys of Iron: An Elementary Introduction. Pergamon. doi: https://doi.org/10.1016/c2013-0-01893-2

25. Bei, H., Yamamoto, Y., Brady, M. P., Santella, M. L. (2010). Aging effects on the mechanical properties of alumina-forming austenitic stainless steels. Materials Science and Engineering: A, 527 (7-8), 2079–2086. doi: https://doi.org/10.1016/j.msea.2009.11.052

26. Huang, J., Ye, X., Xu, Z. (2012). Effect of Cold Rolling on Microstructure and Mechanical Properties of AISI 301LN Metastable Austenitic Stainless Steels. Journal of Iron and Steel Research International, 19 (10), 59–63. doi: https://doi.org/10.1016/s1006-706x(12)60153-8